Catalysis Today 192 (2012) 104–111

Contents lists available at SciVerse ScienceDirect

Catalysis Today

journal homepage: www.elsevier.com/locate/cattod

Niobia-modified aluminas prepared by impregnation with niobium peroxo complexes for dimethyl ether production

Angela S. Rocha[a,b], Aline M. da S. Forrester[a], Elizabeth R. Lachter[a], Eduardo F. Sousa-Aguiar[c], Arnaldo C. Faro Jr.[a,*]

[a] Instituto de Química, Universidade Federal do Rio de Janeiro, Ilha do Fundão, CT, Rio de Janeiro, RJ CEP 21949-900, Brazil
[b] NUCAT/PEQ/COPPE/Universidade Federal do Rio de Janeiro, Caixa Postal 68502, CEP 21941-972, Rio de Janeiro, RJ CEP 21949-900, Brazil
[c] CENPES/Petrobras, Ilha do Fundão, Cidade Universitária, Quadra 7, Rio de Janeiro 21949-900, Brazil

ARTICLE INFO

Article history:
Received 31 October 2011
Received in revised form
29 December 2011
Accepted 9 February 2012
Available online 7 May 2012

Keywords:
Alcohol dehydration
Dimethylether
Syngas
Niobia
Alumina

ABSTRACT

Use of a water-soluble niobium peroxo complex allowed the preparation of niobium-modified aluminas containing up to 90% of the theoretical niobia monolayer in one impregnation step. There was a maximum in the density of surface Lewis acid sites at 45% of the theoretical monolayer. FTIR of adsorbed pyridine and adsorbed CO_2 suggest the vertical growth of the Nb_2O_5 layer for the largest niobium contents. The addition of 22.5% of the theoretical monolayer eliminated about 80% of the basic surface hydroxyls, inhibiting the adsorption of gas phase CO_2 by the samples. The niobia/alumina catalysts suffered less inhibition by CO_2 than the pure alumina in the methanol dehydration reaction, confirming that Nb_2O_5 is mainly deposited on sites where the CO_2 adsorption is stronger, leaving free sites that are active in catalytic dehydration and less inhibited by CO_2, however none of the niobia/aluminas was more active than the pure alumina. Nevertheless, in the direct syngas to DME conversion using a mixed catalyst system comprised of a CuZnAl methanol synthesis catalyst and a methanol dehydration component, the activity was significantly larger with a niobia/alumina as a dehydrating component than with the pure alumina.

1. Introduction

Interest on dimethyl ether (DME) production has grown significantly in recent years, due to its potential use as an alternative fuel to LPG (liquefied petroleum gas) and diesel [1–3], or as an important intermediate in the production of dimethyl sulfate, methyl acetate and light olefins [3]. As a fuel, its use is particularly attractive due to its high cetane number and storage facility. Diesel motors could burn DME after some small modifications, reaching low particulates (soot) and NO_x emission, and no sulfur compounds.

Syngas ($CO + H_2$) is the main source for DME production. This is an additional attractive feature of DME utilization, as syngas can be produced from both natural gas and biomass. DME may be obtained from syngas in one or two steps. The usual process goes through two steps, where methanol is first produced from syngas ($CO + H_2$) and then dehydrated to DME:

$$CO + 2H_2 \rightarrow CH_3OH \quad (1)$$

$$2CH_3OH \rightarrow CH_3OCH_3 + H_2O \quad (2)$$

Methanol synthesis is performed on $CuO–ZnO–Al_2O_3$ based catalysts with high activity and selectivity [4–6], while alcohol dehydration takes place on acid catalysts [7–9]. γ-Alumina is the traditional catalyst for dehydration of alcohols.

An alternative route is the coupled synthesis of methanol and DME from synthesis gas using dual catalyst systems in one step, the so-called STD (synthesis gas to DME) process. In this system, the catalysts could be a physical mixture of the methanol synthesis catalyst and an acid solid or a bi-functional catalyst with activity to produce methanol, and also dehydrate methanol to DME and water [3,10–17]. Besides reactions (1) and (2) above, reaction (3) below, the water-gas shift (WGS) reaction, also occurs in this system, as the normally used methanol synthesis catalyst (CuZnAl) is also active for the WGS reaction:

$$CO + H_2O \rightarrow CO_2 + H_2 \quad (3)$$

γ-Alumina would be a natural choice as a dehydrating component in such a dual catalyst system. However, previous work from our group with alumina-supported niobia in isopropanol dehydration [18] highlighted the importance of basic sites for this reaction. In fact, in the case of alumina-supported niobia, a linear correlation was found between the specific isopropanol dehydration activity and basic site density. The fact that carbon dioxide adsorbs strongly

* Corresponding author. Tel.: +55 21 25627821.
E-mail addresses: farojr@iq.ufrj.br, farojr@gmail.com (A.C. Faro Jr.).

0920-5861/$ – see front matter © 2012 Elsevier B.V. All rights reserved.
http://dx.doi.org/10.1016/j.cattod.2012.02.062

on basic sites (it is frequently used as a probe molecule for basic site titration) is a potential problem for this use of alumina, since considerable amounts of carbon dioxide are produced by reaction (3) in the STD process.

Previous work has shown that deposition of niobia on the alumina surface leads to the elimination of basic sites [18,19]. On one hand, this had a negative effect on the isopropanol dehydration reaction [18] but, on the other, it also inhibited carbon dioxide adsorption. A balance between these effects could lead to an improved performance of niobia–alumina, as a dehydration component in dual catalyst systems for DME production, as compared to pure γ-alumina.

In this paper, we report on the effect of supported niobia on the activity and selectivity of γ-alumina in DME production, as a dehydration component in a dual catalyst system for the STD process. We also present results on the activity of these materials in the gas phase methanol dehydration reaction and on the inhibitory effects of carbon dioxide on this activity.

In the preparation of niobia/alumina catalysts, it is difficult to introduce high amounts of niobia in one impregnation step, because generally the niobia precursors have low solubility in water. It has been recently reported that niobium peroxo complexes have a high water solubility [20] and appear to be an attractive alternative for the preparation of supported catalysts with high niobium loadings in a single impregnation step. So we also present results on the characterization of niobia/aluminas prepared from ammonium diperoxo-dioxaloniobate.

2. Experimental

2.1. Catalysts preparation

The γ-alumina was obtained by calcination of a commercial boehmite supplied by Condea Chemie (Pural SB RT04/111) at 823 K for 3 h. Bulk niobium oxide was prepared by calcination at 773 K for 4 h of niobic acid ($Nb_2O_5{\cdot}nH_2O$), supplied by CBMM (Araxá, Brazil).

The niobium precursor used was the ammonium diperoxo-dioxalo niobate complex $(NH_4)_3[Nb(O_2)_2(C_2O_4)_2]$, that was synthesized in two steps using the method reported by Bayot et al. [20]. First, the synthesis of ammonium tetraperoxoniobate, $(NH_4)_3[Nb(O_2)_4]$, was performed by treatment of 1 g of niobic acid in 25 mL of distilled water with 25 mL of a 30 wt% solution of H_2O_2 and 6 mL of 25 wt% solution of ammonia. The mixture was agitated until complete dissolution, when 50 mL of acetone were added, yielding a white precipitate, which was filtered off, washed with acetone and air-dried. This first complex was dissolved in an aqueous oxalic acid solution. The solution turns rapidly to a bright yellow color. Addition of acetone yielded a yellow microcrystalline solid, the niobium precursor, which was filtered off, washed with acetone and air-dried.

Four Nb_2O_5/Al_2O_3 catalysts, containing between 22.5 and 90.1% of the theoretical monolayer (6.3 niobium atoms per nm^2 [21]) of niobia on alumina (between 5.9 and 20 wt%), were prepared by incipient wetness impregnation of a γ-alumina obtained from boehmite by calcination at 823 K with a solution containing the required amount of the niobium precursor complex dissolved in 10 wt% aqueous nitric acid. The catalysts were subsequently dried at 393 K for 2 h and calcined at 723 K for 4 h. In preliminary tests (not shown here for reasons of space) where the calcination temperature was varied between 623 and 773 K, a maximum in catalytic activity for methanol dehydration was found for this temperature. These samples were named *X*%NbAl, where *X* is the niobia content in wt%.

A commercial methanol synthesis catalyst supplied by Johnson Matthey Catalysts (KATALCO 51-9), named here CuZnAl, was used without modification as the methanol synthesis component in the mixed catalyst system. A γ-Al_2O_3 calcined at 773 K for 3 h or 11.1%NbAl were used as the dehydration component.

2.2. Characterization

The surface areas and pore volumes of all catalysts were determined from nitrogen adsorption data at 77 K in an automated volumetric apparatus, Micromeritics ASAP 2010 C. Before the analyses all samples were treated in situ under vacuum at 673 K. The catalysts were analyzed by X-ray diffraction in a Rigaku Miniflex diffractometer, with Cu Kα radiation, λ = 1.5418 Å, 30 kV and 15 mA.

FTIR measurements were carried-out in a Perkin Elmer Spectrum One spectrophotometer, between 4000 and 400 cm^{-1}. Self-supported wafers of the samples, containing 10 mg cm^{-2}, were evacuated at ca. 1.3 mPa (10^{-5} Torr) and 723 K for 4 h. After cooling to room temperature, the spectrum was recorded. For the acidity analysis, the sample at 323 K was then exposed to 0.133 kPa (1 Torr) of pyridine vapors at equilibrium and a second spectrum was recorded. The same wafer was submitted to evacuation for 10 min at 323 K and the spectrum was obtained. Subsequent evacuation was performed at 373, 423, 473, 573 and 673 K for 10 min followed by the spectral acquisitions. The spectra presented were obtained by subtracting the spectra recorded after from the one recorded before pyridine introduction. For the basicity analysis, essentially the same procedure was followed, replacing the pyridine by CO_2.

2.3. Methanol dehydration in a recirculation system

Methanol dehydration experiments were performed at 101 kPa total pressure, 523 K and 8.9 kPa methanol initial partial pressure (balance helium) in a batch apparatus with external re-circulation of the gas phase. The re-circulation loop is connected to a vacuum line that can be evacuated to ca. 1.3 mPa (10^{-5} Torr). About 10 mg of catalyst were used after in situ evacuation at 723 K. In a similar series of experiments, carbon dioxide was added to the reactant in a 1:1 proportion relative to methanol.

The composition of the reaction mixture was measured by periodically withdrawing samples from the gas phase and injecting them into a gas chromatograph (HP 6890) equipped with a methyl siloxane capillary column (100.0 m × 250 μm × 0.50 μm) and a mass-selective detector (MSD HP 5973). Under the applied reaction conditions, the only observed product was DME. Activities were calculated from the initial slope of conversion vs. time data.

2.4. Direct synthesis of DME in a batch reactor

The catalytic systems, comprised of a physical mixture of 2 g of a commercial methanol synthesis catalyst (CuZnAl) and 4 g of a methanol dehydration catalyst (γ-Al_2O_3 or Nb_2O_5/Al_2O_3), was suspended in n-hexadecane and evaluated in the direct synthesis of dimethyl ether from syngas (CO/H_2 1:2 molar ratio) in a high pressure batch reactor.

A Parr commercial reactor, model 4560, equipped with a gas burette, was modified for the catalytic measurements. The catalysts were pre-treated in situ with 200 mL min^{-1} of hydrogen at 5.0 MPa, 533 K for 16 h, with heating rate of 10 K min^{-1}. After reduction, the reactor was depressurized, purged with the syngas, the temperature was raised to 553 K under agitation of 500 rpm and pressurized to 5.0 MPa. The gas burette was previously adjusted to keep the system at 5.0 MPa during the reaction and the syngas uptake was obtained by the decrease in pressure in the gas burette.

After consumption of 1.0 MPa of syngas from the burette, a gas phase sample was removed from the reactor and analyzed in the same gas chromatograph described under Section 2.3. Under

Table 1
Textural characterization of the alumina and niobia/aluminas.

Catalyst	A[a] ($m^2\ g^{-1}$)	A_{corr}[b] ($m^2\ g^{-1}$)	V_P[c] ($cm^3\ g^{-1}$)	V_{corr}[d] ($cm^3\ g^{-1}$)	d_P[e] (nm)
γ-Al_2O_3	199	199	0.58	0.58	11.6
5.9% NbAl	197	209	0.54	0.57	11.0
11.1% NbAl	188	211	0.50	0.56	10.6
15.9% NbAl	186	221	0.47	0.56	10.1
20% NbAl	184	230	0.43	0.54	9.3

[a] Surface area per mass of catalyst.
[b] Surface area per mass of support.
[c] Pore volume per mass of catalyst.
[d] Pore volume per mass of support.
[e] Average pore diameter from $4V_P/A$.

the conditions used here, the detectable gas phase products were methanol, DME, carbon dioxide and water. The n-hexadecane phase was also analyzed for the identification of any heavy products that might be formed in the reaction, but no products could be detected.

Activities were obtained from change in pressure vs. time data, which were transformed into molar quantities using compressibility factors. Selectivity measurements were performed at iso-conversion by means of the chromatographic analysis. Negligible quantities of ethane were also observed.

3. Results and discussion

3.1. Identification of the ammonium diperoxo-dioxaloniobate complex

The niobium peroxo-oxalate complex used in the synthesis of all niobia/alumina was identified by FTIR using KBr wafer. The spectrum is available as supporting information. The main bands observed are assigned in accordance with the proposals of Bayot et al. [20] for this type of complex. Thus, the asymmetric stretching frequency of the carboxylate groups complexed to niobium appears as a not well defined band at 1685 cm^{-1} and a symmetric mode band appears around 1400 cm^{-1}. The bands at 1707 and 1257 cm^{-1} are attributed to C═O and C—O stretching modes. The terminal Nb═O vibration could be identified by the band at 909 cm^{-1}. Diperoxo species present bands in the region of 800–880 cm^{-1}.

The obtained complex was calcined at 873 K for 4 h and lost 29.9% of its initial weight, against an expected loss of 30.7% according to the reaction expected from decomposition of ammonium diperoxo-dioxalo niobate:

$$2(NH_4)_3[Nb(O_2)_2(C_2O_4)_2] \rightarrow 6NH_3 + 8CO_2 + 3H_2O + Nb_2O_5$$

The solubility of the complex was found to be 0.226 g mL^{-1} in water (niobium oxide basis) and 0.385 g mL^{-1} in 10 wt% HNO_3 solution (also niobium oxide basis). With these high values of solubility, it was possible to prepare all the niobia/alumina materials using only one incipient wetness impregnation step. For comparison, the water solubility of ammonium oxaloniobate, commonly used as a precursor for aqueous impregnation of niobium, was ca. 0.15 g mL^{-1}, niobium basis.

3.2. Characterization of niobia/aluminas with varying niobium contents

For all alumina-supported niobia catalysts, X-ray diffraction patterns only displayed the characteristic reflections of the γ-alumina support. Analysis by X-ray fluorescence provided results for the niobium contents that differed by less than 7% from the theoretical ones. The niobia loadings used here are the ones obtained from XRF, not the nominal ones.

Textural properties (surface areas, pore volumes and average pore diameters) are shown in Table 1. Surface areas and pore volumes, on a catalyst mass basis, decreased slightly with increasing niobium loading. Even if pore blockage did not occur, some decrease in these values is expected simply from the increase in density of the materials due to niobium incorporation. To correct for this factor, surface areas per mass of support are also presented in Table 1. Interestingly it is seen that corrected surface areas actually increase significantly with increasing niobium content. At the same time, corrected pore volumes and average pore diameters, calculated from $4V/A$, decrease in the same direction. If a porous amorphous niobia phase was formed, separate from the alumina phase, one would expect an increase, and not the observed decrease in the corrected pore volume. Thus it seems that the supported niobia phase is deposited inside the pores of the alumina, causing a decrease in pore volume and in pore diameter, but increasing the surface area per mass of support, presumably due to a roughening of the surface.

The FTIR spectra of the pure and niobia-modified aluminas in the OH-stretching region, after evacuation at 723 K for 4 h, are shown in Fig. 1. Peak maxima are observed with the pure alumina at 3770, 3730, 3675 and 3587 cm^{-1}. Maxima close to these wavenumbers have been attributed to hydroxyl groups of increasing basicity as the wavenumber increases [19,22,23]. The assignment of these bands has been discussed before [22–25]. With the niobia-modified aluminas it is clearly seen that the three maxima with the highest wavenumbers decrease pronouncedly as the niobium content increases. The profiles obtained are very similar to the ones reported by Burcham et al. [19], except that, here, the peak at 3770 cm^{-1}, corresponding to the most basic surface hydroxyls, cannot be discerned already at a niobium content corresponding to 22.5% of the theoretical monolayer (5.9 wt% niobia).

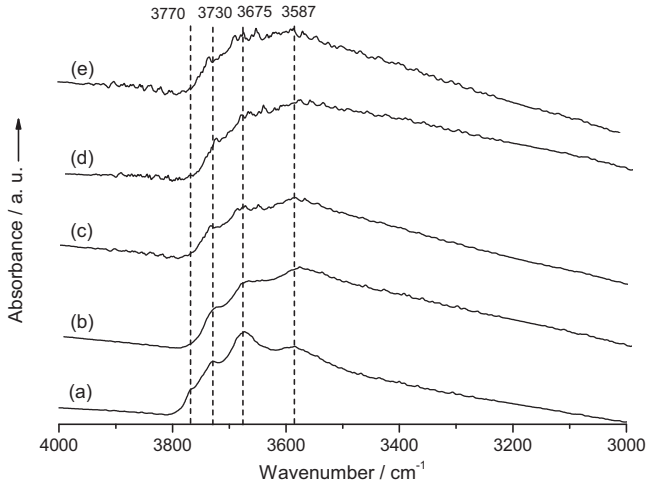

Fig. 1. FTIR spectra in the OH stretching region. (a) γ-Al_2O_3; (b) 5.9%NbAl; (c) 11.1% NbAl; (d) 15.9%NbAl; (e) 20%NbAl.

Table 2
Amount of pyridine adsorbed on Lewis acid sites as a function of temperature.

Temperature	Catalyst				
	γ-Al_2O_3	5.9%NbAl	11.1%NbAl	15.9%NbAl	20%NbAl
	Pyridine adsorbed on Lewis sites				
423[a]	117	110	134	107	130
473[b]	84	75	91	85	80
573[b]	57	28	57	48	37
673[b]	10	11	15	11	6.8

[a] Absolute amount in $\mu mol\,g^{-1}$.
[b] Amount relative to the one adsorbed at 423 K.

Table 3
Integrated FTIR peak areas for the bands associated with pyridine adsorbed on aluminum (1623 and 1617 cm^{-1}) and niobium (1610 cm^{-1}) Lewis acid sites vs. niobium loading as percentage of the theoretical monolayer (evacuation at 423 K for 10 min).

Catalyst	Integrated peak areas (a.u.)			% T.M.[d]
	$A_{1623}+A_{1617}$ [a]	A_{1610} [b]	% A_{1610} [c]	
γ-Al_2O_3	1.03	0.00	0.0	0.0%
5.9%Nb/Al	0.57	0.21	26.5	22.5%
11.1%Nb/Al	0.54	0.76	58.4	45.0%
15.9%Nb/Al	0.40	0.57	58.5	67.5%
20%Nb/Al	0.51	0.59	53.6	90.1%

[a] Added integrated peak areas for the bands at 1623 and 1617 cm^{-1}.
[b] Integrated peak area for the band at 1610 cm^{-1}.
[c] Integrated peak area for the band at 1610 cm^{-1} relative to the added area of the three bands.
[d] Niobia loading as percentage of the theoretical monolayer (6.3 Nb atoms per nm^2).

The acidities of the materials were studied by FTIR of adsorbed pyridine after evacuation at different temperatures. Spectra obtained after evacuation at 423 K for 10 min are shown in Fig. 2. Absorbances were obtained after subtraction of the spectrum from the dried wafer before pyridine adsorption.

The usual bands attributed to pyridine adsorbed on Lewis acid sites (LAS) are observed on all catalysts in the region of 1600–1625 cm^{-1} (ν_{8a} C—C), 1575 cm^{-1} (ν_{8b} C—C), 1490 cm^{-1} (ν_{19a} C—N) and 1450 cm^{-1} (ν_{19b} C—N). Analyzing the group of bands attributed to ν_{8a} C—C, it is possible to observe differences among the samples with varying niobia contents. While this band appears as a doublet around 1617 and 1623 cm^{-1} in the alumina spectrum, a band around 1610 cm^{-1} appears as a shoulder that increases with the niobia content. This band has already been reported as pyridine coordinated to co-ordinatively unsaturated Nb^{5+} sites in niobium phosphate [26] and niobia/alumina [18].

A small band at 1540 cm^{-1}, attributed to pyridine adsorbed on Brønsted acid sites, is observed only in the spectrum of 20%NbAl. This result indicates the incipient formation of three-dimensional particles of niobia dispersed on alumina, in the catalyst with the highest niobia content.

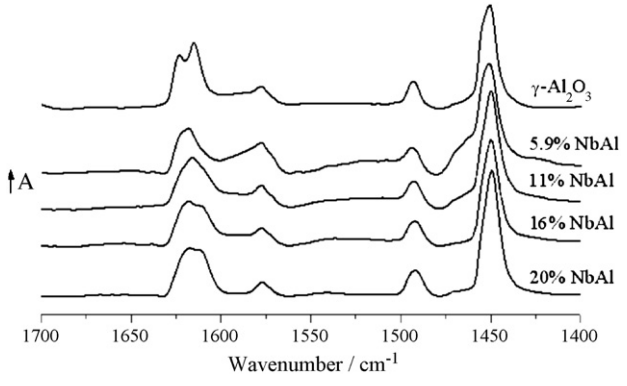

Fig. 2. FTIR spectra of adsorbed pyridine after evacuation at 423 K on the NbAl catalysts.

Quantification of the LAS was obtained from the spectra of adsorbed pyridine using the method proposed by Emeis [27]. Table 2 summarizes the results of such quantification. The figures for the 423 K evacuation temperature correspond to the amount of pyridine adsorbed on the LAS. For the remaining temperatures, the figures represent the fraction of pyridine remaining on the LAS after evacuation at a given temperature. No systematic variation in total Lewis acidity was found as a function of niobium loading, all values lying near to $120 \pm 14\,\mu mol\,g^{-1}$. However, a maximum acidic strength appears to exist for the catalyst containing 11.1% niobia (45% of the theoretical monolayer, assuming monolayer coverage to be 6.3 Nb atoms per nm^2 [21]), since this catalyst retained the largest fraction of the LAS-adsorbed pyridine after evacuation at 673 K. Several studies [28–30] use the concept of cation electronegativity in order to explain the increase in acid strength of oxides with addition of a dopant: the acid strength of the oxide is thought to be increased upon addition of a more electronegative cation, due to inductive effects. Using the method proposed by Tanaka and Osaki [28] for the calculation of electronegativities, values of 17.6 and 10.5 are obtained for Nb^{5+} and Al^{3+}, respectively. The increase in acid site strength when niobia partially covers the alumina surface may therefore be related to the increase in acid strength of weaker acidic sites on the alumina surface, caused by the inductive effect of neighboring niobium atoms. The subsequent decrease may be due to coverage of these LAS by niobia as suggested by the growth of the band at 1610 cm^{-1} with increasing niobium content.

The group of bands between 1600 and 1625 cm^{-1} was decomposed, using Lorentzian functions, into three constituent bands, one of them at ca. 1610 cm^{-1}, assumed to arise from pyridine adsorbed on niobium LAS, and two others at ca. 1617 and 1623 cm^{-1}, respectively, attributed to pyridine adsorbed on aluminum LAS [18]. Fig. 3 illustrates the results of these decompositions.

The existence of two 8a vibration bands with alumina may be attributed to pyridine adsorbed on octahedrally (1617 cm^{-1}) and tetrahedrally (1623 cm^{-1}) coordinated Al^{3+} ions [31]. The

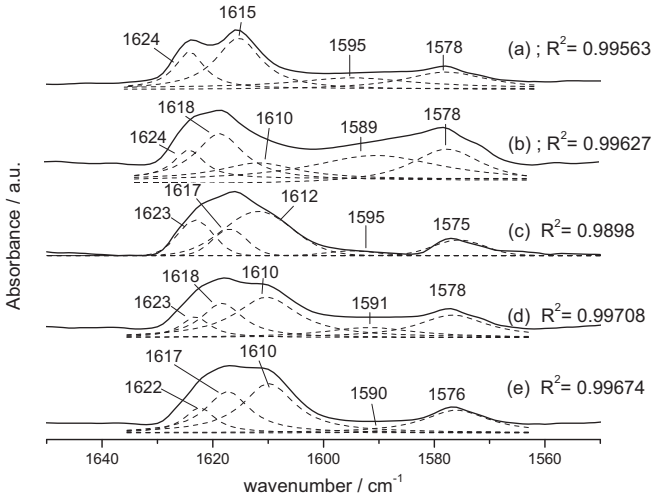

Fig. 3. Deconvolution of the FTIR bands of adsorbed pyridine in the range 1550–1650 cm^{-1}. (a) γ-Al_2O_3; (b) 5.9%NbAl; (c) 11.1%NbAl; (d) 15.9%NbAl; (e) 20%NbAl.

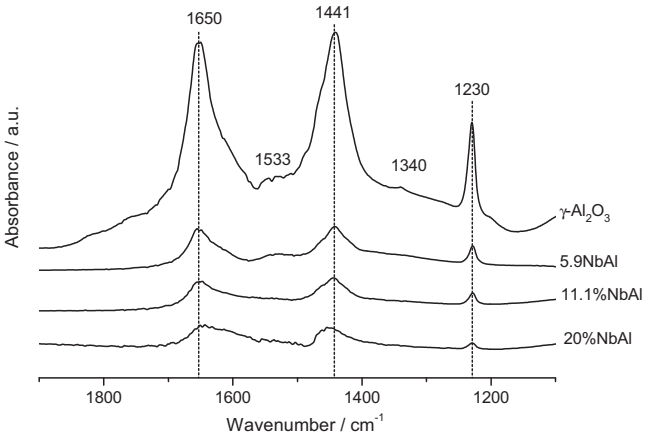

Fig. 4. FTIR spectra of adsorbed carbon dioxide after evacuation at 323 K.

integrated intensities of these bands, per unit catalyst area, after evacuation at 423 K, are shown in Table 3. The intensities of the bands at ca. 1617 and 1623 cm^{-1} were added, in order to obtain a number proportional to the surface concentration of pyridine adsorbed on aluminum LAS. Assuming molar extinction coefficients to be the same for the bands assigned to pyridine adsorbed on aluminum sites and the one for pyridine adsorbed on niobium sites, the proportion of pyridine adsorbed on niobium sites may be estimated. From the last column in Table 3, it is seen that the percentage of pyridine adsorbed on niobium LAS follows quite closely the niobium content in terms of percentage relative to the theoretical monolayer, up to a niobia loading corresponding to nearly 60% of the theoretical monolayer. This suggests that, up to this point, the niobia is spread essentially as a monolayer on the surface of the alumina.

Chemisorption of CO_2 has been used as a probe for basic sites on solid surfaces [32]. While γ-Al_2O_3 is capable to chemisorb this probe molecule, no chemisorption could be observed for pure niobia, which indicates the absence of basic sites on the niobia surface. In this paper, carbon dioxide chemisorption on alumina and on the niobia/aluminas was followed by FTIR spectroscopy. After the initial evacuation at 673 K, all materials presented strong absorption bands at 1476 and 1569 cm^{-1}. The small separation between the peaks and the fact that these bands resist evacuation up to 673 K suggest that they arise from a bulk carbonate, rather than from un-removed adsorbed carbon dioxide [32]. All spectra shown after carbon dioxide chemisorption and subsequent evacuation are difference spectra relative to each material after evacuation at 673 K and before carbon dioxide chemisorption.

Fig. 4 shows the spectra obtained for γ-alumina and the niobia/aluminas after carbon dioxide chemisorption and subsequent evacuation at 323 K for 10 min. In the region of 1100–1900 cm^{-1}, the most important bands are observed at 1230, 1441 and 1650 cm^{-1}. Bands near these values have been assigned by Baltrusaitis et al. [33], respectively, to the δ_4(COH), $\nu_3(OCO)_s$ and $\nu_2(OCO)_a$ vibration modes of adsorbed bicarbonate. From isotopic labeling experiments and quantum mechanical calculations, these authors propose that carbon dioxide chemisorption on surface hydroxyls leads to the formation of a bridge-bonded bicarbonate species. The intensity of these bands decrease strongly, even for a niobium loading corresponding to only 22.5% of the theoretical monolayer, confirming that niobia titrates preferentially the basic hydroxyl groups of the alumina surface, as reported before in the literature [18,19].

Besides these main bicarbonate bands, shoulders can be observed in the spectrum of the alumina support (cf. Fig. 5) at the low wavenumber side of the ν_2 vibration mode and the high wave number side of the ν_3 vibration mode. These shoulders may be attributed to another type of surface bicarbonate. According to the calculations of Baltrusaitis et al. [33], the difference in wavenumber between the ν_2 and ν_3 vibration modes would be smaller in a bidentate surface bicarbonate species than for a bridge-bonded one. Clearly these shoulders become relatively more important as the niobia loading increases. It is reasonable to expect that, as the coverage of the alumina surface by niobia increases, the probability of formation of a bridge-bonded bicarbonate species, that requires two aluminum atoms, decreases with respect to the formation of a bidentate one, that requires a single aluminum atom.

Besides these shoulders, small and broad bands can also be observed at ca. 1530 and 1350 cm^{-1}, which are especially evident in the spectrum of the γ-alumina support. As discussed by Lavalley [32], the free carbonate anion has a ν_3 vibration mode at 1415 cm^{-1} and loss of the D_{3h} symmetry on adsorption leads to splitting of these band, producing a doublet symmetrically located around 1415 cm^{-1}. The average between 1350 and 1530 is close to 1415, so these bands are consistent with adsorbed carbonate, however there is not a general agreement on the assignment of this band to a specific adsorption mode [32,34]. These bands also

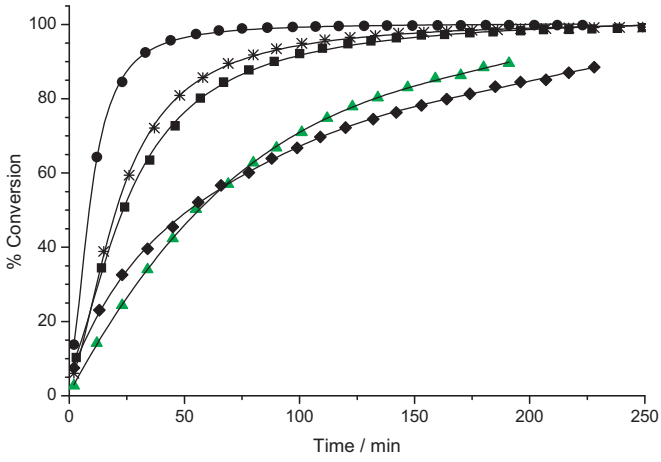

Fig. 5. Kinetic curves for methanol dehydration (373 K, 8.9 kPa methanol initial pressure, 10 mg catalyst). ●, γ-Al_2O_3; ✳, 5.9%NbAl; ■, 11.1%NbAl; ♦, 15.9%NbAl; ▲, 20%NbAl.

Table 4
Integrated peak areas for the 1230 cm^{-1} band (bicarbonate) of adsorbed CO_2 normalized by catalyst mass.[a]

Temperature (K)	Catalyst			
	Alumina	5.9%NbAl	11.1%NbAl	20%NbAl
	% Theoretical monolayer			
	0	22.5	45.0	90.1
(Ads CO_2)[b]	2.82	0.57(0.20)	0.41(0.15)	0.22(0.08)
323[c]	1.49	0.24 (0.16)	0.15 (0.1)	0.06 (0.04)
373[c]	0.61	0.07 (0.11)	0.02 (0.04)	0.01 (0.02)
423[c]	0.24	0.02 (0.08)	0.02 (0.07)	0.003 (0.01)

[a] Numbers between brackets represent the mass normalized peak area relative to that of the pure alumina under the same conditions.
[b] In the presence of 0.133 kPa (1 Torr) CO_2 at room temperature.
[c] After evacuation for 10 min at the specified temperature.

decrease in intensity as the niobium loading increases, in line with the expectation that the surface basicity decreases as the coverage of the alumina surface by niobia increases.

The intensity of the δ_4(COH) band at 1230 cm^{-1} may be taken as a measure of the concentration of basic hydroxyl groups at oxide surfaces [32]. In Table 4 are reported the peak areas per unit surface area for several catalysts both in the presence of 0.133 kPa (1 Torr) CO_2 and after evacuation at different temperatures. For the niobia/aluminas, the values between brackets represent the normalized peak areas as a fraction of the one obtained with the pure alumina under the same conditions. In the presence of 0.133 kPa CO_2, the amount adsorbed on the catalysts decrease with increasing niobium loading and, on the catalyst containing a niobia loading corresponding to 22.5% of the theoretical monolayer (5.9%NbAl), the amount of adsorbed CO_2 is already only 20% of the amount adsorbed on the pure alumina, confirming that niobia titrates preferentially the hydroxyl groups responsible for carbon dioxide adsorption, i.e., the basic hydroxyl groups. With increasing evacuation temperature, this effect is intensified, so that after evacuation at 423 K, the carbon dioxide amount remaining on 5.9%NbAl is only 8% of the one remaining on the pure alumina under the same conditions. A similar effect is observed with the higher niobium loadings. This shows that the basic hydroxyls remaining on the uncovered portion of the niobia/alumina surface are not only fewer but also weaker than the ones originally present on the alumina.

3.3. Gas phase methanol dehydration

The only reaction products observed in methanol dehydration on alumina and niobia/aluminas were DME and water up to 573 K reaction temperature. With the most active catalyst, which was the pure alumina, at 523 K equilibrium conversion was reached after ca. 50 min reaction time and no secondary products could be observed after 4 h reaction. In order to illustrate the type of data obtained in this work, Fig. 5 shows kinetic curves for methanol dehydration obtained at 523 K.

The methanol dehydration activities determined from the initial rates of reaction for all catalysts, both in presence and in the absence of added carbon dioxide in a 1:1 ratio to methanol, are presented in Table 5. Without carbon dioxide addition, there is a nearly 60% decrease in activity with respect to the pure alumina upon adding 5.9% niobia. However, in the series of niobia/aluminas a maximum in activity occurs with 11.1%NbAl.

The strong decrease in activity upon supporting niobia on the alumina surface may be ascribed to titration of the strongest alumina basic sites by niobia, as revealed by the adsorbed CO_2 FTIR spectra. Previously we demonstrated that activity for isopropanol dehydration correlates linearly with the basic site concentration of pure and niobia-modified alumina, as measured by CO_2 chemisorption. Both olefin and ether formation are influenced in the same direction, but olefin formation is more affected. Schiffino

Table 5
Initial reaction rates for methanol dehydration (373 K, 8.9 kPa methanol initial pressure, 10 mg catalyst).

Catalyst	Reaction rates (mmol g^{-1} min^{-1})		Ratio[c]
	Without CO_2 [a]	With CO_2 [b]	
γ-Al_2O_3	14.1	5.2	0.37
5.9%NbAl	5.2	3.1	0.60
11.1%NbAl	8.1	4.1	0.51
15.9%NbAl	4.3	3.4	0.71
20%NbAl	3.1	1.6	0.52

[a] Without added CO_2.
[b] CO_2 added to the reactant in a 1:1 ratio to methanol.
[c] Ratio of the two reaction rates.

and Merrill [35] have proposed that methanol dehydration on alumina may occur through two paths, one involving reaction between two adsorbed methoxides and the other involving the reaction between an adsorbed methoxide and a methanol molecule hydrogen-bonded to the surface, with the latter predominating at temperatures below 553 K. This mechanism may be represented by Scheme 1 below, where Al^+ represents a Lewis acid site and OH a basic surface hydroxyl group:

In this mechanism, alkoxide formation requires methanol dissociative chemisorption on an acid–base pair. According to the results in Table 2, deposition of 5.9% niobia does not strongly affect concentration or strength of the Lewis acid sites. However, the results in Table 4 demonstrate that basic hydroxyls are strongly affected by niobia deposition. The strong decrease in activity parallels the decrease in basic hydroxyl concentration. On the other hand, the results in Table 4 show that, after the 5× decrease upon the addition of 5.9% niobia, the basicity decreases more slowly with increasing niobia loading. The fact that the activity decreased by a factor of about 3, while the concentration of basic hydroxyl groups decreased by a factor of about 5 (cf. 4th row in Table 4) upon addition of 5.9 wt% niobia to the alumina, may be explained if basic surface sites other than hydroxyls, such as oxide anions, may also participate in the reaction. It should be noticed that bands that can

$$CH_3OH + Al^+\text{-}OH \rightarrow CH_3O\text{-}Al\text{-}OH_2^+$$

$$CH_3O\text{-}Al\text{-}OH_2^+ \rightarrow CH_3O\text{-}Al^+ + H_2O$$

$$CH_3O\text{-}Al^+ + CH_3OH\text{---}OH\text{-}Al^+ \rightarrow (CH_3)_2O\text{---}Al^+\text{-}OH + Al^+\text{-}OH$$

$$(CH_3)_2O\text{---}Al^+\text{-}OH \rightarrow (CH_3)_2O + Al^+\text{-}OH$$

Scheme 1.

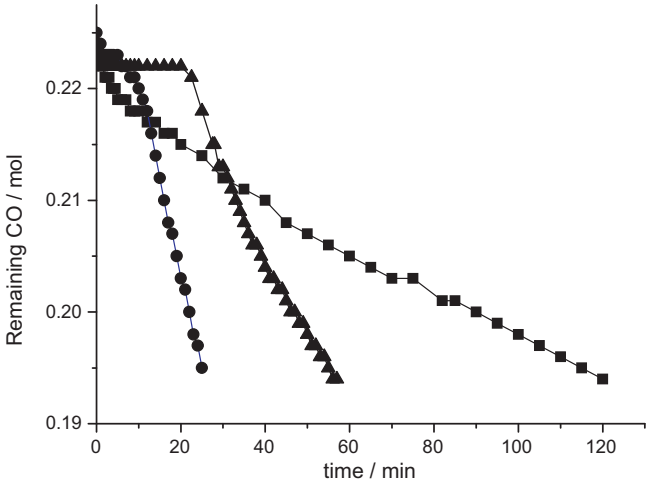

Fig. 6. Carbon monoxide uptake during syngas conversion (553 K, 5.0 MPa, 2 g methanol synthesis catalyst, 4 g methanol dehydration catalyst). ■, CuZnAl; ▲, CuZnAl + γ-Al_2O_3; ●, CuZnAl + 11.1%NbAl.

be assigned to surface carbonate, i.e., derived from surface oxide rather than from hydroxide anions, were observed in our FTIR spectra of adsorbed CO_2.

The activity maximum observed with 11.1%NbAl appears to be genuine, since it was also observed in a separate series of experiments carried-out with carbon dioxide addition, as shown in the third column in Table 5. This maximum may be related to the maximum in the concentration of Lewis acid sites able to retain adsorbed pyridine up to 673 K, as shown in Table 2.

The initial rate results shown in the last column of Table 5 confirm the importance of the basic sites in methanol dehydration on γ-alumina and the niobia/aluminas, as addition of carbon dioxide in a 1:1 proportion to methanol strongly inhibited the reaction, especially on alumina, where the rate in the presence of carbon dioxide was approximately 1/3 of the rate in its absence. Although carbon dioxide also inhibited the reaction on the niobia/aluminas, the extent of inhibition was considerably smaller than in the case of the pure alumina. This may be explained by the fact that niobia titrates preferentially the strongest basic sites on the alumina surface, that adsorb carbon dioxide more strongly.

This is expected to have an important impact in the use of these catalysts in hybrid catalyst systems for the direct syngas to DME conversion, as the main overall reaction occurring in this system is reaction (4) below:

$$3CO + 3H_2 \rightarrow CH_3{-}O{-}CH_3 + CO_2 \quad (4)$$

The large amount of carbon dioxide produced may lead to strong competition with methanol for the basic sites involved in methanol dehydration. It should be noticed, however, that, under the conditions used here, the smaller inhibition by carbon dioxide of methanol dehydration on the niobia/aluminas was not capable of offsetting the decrease in activity derived from niobia deposition on the alumina surface.

3.4. Direct synthesis of DME

Some preliminary results on the use of a mixed catalyst system comprised of a commercial methanol synthesis catalyst and 11.1%NbAl, the most active NbAl methanol dehydration catalyst, are shown in Fig. 6. The curves represent the amount of CO remaining in a gas burette filled with syngas with a 2:1 H_2/CO molar ratio connected, via a pressure regulator, to the reactor containing the catalyst system suspended in n-hexadecane, as described in detail under Section 2.4. The amount of remaining CO was calculated from the decrease in pressure in the gas burette, assuming that the 2:1 H_2/CO ratio remained constant in the burette throughout the experiment.

Table 6
Rate of carbon monoxide uptake during syngas conversion on single and mixed catalyst systems (553 K, 5.0 MPa, 2 g methanol synthesis catalyst, 4 g methanol dehydration catalyst).

Dehydration catalyst	Consumption rate[a] ($\times 10^3$/mol min^{-1} g^{-1})
–	0.34
Al_2O_3	1.02
11.1% NbAl	3.01

[a] Rate obtained considering only the weight of the methanol synthesis catalyst.

It is clear from Fig. 6 that, without the dehydration component, the rate of syngas consumption initially decreases, but subsequently attains a nearly steady behavior in terms of syngas consumption vs. time. When the pure γ-alumina was used as the dehydration component, an initial induction time is observed during which the rate of reaction is very slow, but subsequently it becomes much larger than the one obtained with the methanol synthesis catalyst alone. With 11.1%NbAl as the dehydration component, the induction period is significantly less pronounced and the rate of syngas consumption is larger than obtained with γ-alumina as the dehydration component. Furthermore, from the curvature of the remaining CO vs. time curves, there appears to be a smaller decrease in the rate of carbon monoxide consumption as the reaction proceeds.

From the slopes of the linear portion of the remaining CO vs. time curves, catalyst activities were established and are shown in Table 6. All of the activity values are referred to the mass of the methanol synthesis catalyst used in the experiments. It is found that the overall activity obtained with the niobia/alumina as the methanol dehydration component is ca. three times the one obtained with the pure γ-alumina.

The induction period observed with the mixed catalyst systems may be related to the mechanism of methanol synthesis. Carbon dioxide has been found to be the main reactant in carbon monoxide hydrogenation [12,36,37]. Conversion of carbon monoxide actually occurs mainly through the water gas shift (WGS) reaction, which allows the maintenance of a steady-state concentration of carbon dioxide in the system, as shown in Scheme 2 below:

In the absence of added CO_2, the shift reaction cannot be the path for the initial CO_2 formation. In this case, some CO could be consumed in a Boudouard reaction ($2CO \rightarrow CO_2 + C$) to produce CO_2, as proposed previously [38]. This CO_2 might be enough to initiate methanol synthesis. Once the synthesis reaction is initiated, the water produced in carbon dioxide hydrogenation may help to retard carbon deposition by the Boudouard reaction via a carbon reforming reaction (reaction (5) below):

$$H_2O + C \rightarrow CO + H_2 \quad (5)$$

Thus, the induction period observed here with the mixed catalyst systems may be explained by adsorption of water and carbon dioxide by the dehydration component of the system. The smaller induction period observed with the niobia/alumina catalyst would then result from the inhibition of water and carbon dioxide adsorption by the surface niobia.

$$CO_2 + 3H_2 \rightarrow CH_3OH + H_2O$$

$$CO + H_2O \rightarrow CO_2 + H_2$$

Scheme 2.

In the direct synthesis of DME from syngas, the water produced in the methanol dehydration reaction is responsible to drive the shift reaction and to maintain a sufficient carbon dioxide concentration level in the system. This explains the much larger overall activity with the mixed catalyst system [12]. Furthermore, removal of water by the WGS reaction helps to increase catalyst life [39].

It is interesting that the activity for DME production of the mixed system CuZnAl plus 11.1NbAl was significantly higher than that of the one with alumina, even though niobium addition causes a reduction of the alumina activity for methanol dehydration. This is likely due to the smaller inhibition of methanol dehydration by carbon dioxide adsorption on the niobia/alumina catalysts than on pure γ-alumina, as reported in Table 5. Although in the gas phase methanol dehydration tests reported here none of the niobia/alumina catalysts was more active than the pure alumina, it is conceivable that in the liquid phase and at the high pressures used in the syngas to methanol experiments the inhibition factor becomes more important than the activity factor.

Selectivity to carbon products (DME, methane and CO_2) are very similar for both mixed systems. Carbon dioxide and DME were produced in approximately 1:1 ratio, showing that the predominant overall reaction is the aforementioned reaction (4). Methanol constitutes 3–4% of the converted carbon monoxide. Therefore, niobia addition to the alumina accelerates the whole reaction cycle, i.e., increased rate of methanol dehydration increases the production of water, which in its turn increases the WGS reaction and consequently the methanol synthesis reaction.

4. Conclusions

The use of a peroxo-oxalo niobium complex allowed the preparation of alumina-supported niobium oxide containing up to 90% of a theoretical monolayer in a single incipient wetness impregnation step. The niobia on these materials was well dispersed, probably as a monolayer at least up to a niobia loading of nearly 60% of the theoretical monolayer.

No systematic trend in total Lewis acidity could be observed as a function of niobium loading, but a maximum in Lewis acid strength was found at a niobia loading around 45% of the theoretical monolayer. Deposition of niobia resulted in a strong decrease in the surface concentration of basic hydroxyl groups and the most basic ones were preferentially eliminated.

Deposition of niobia also resulted in a strong decrease in the activity for methanol dehydration, paralleling the effect on basicity, but an activity maximum was found within the series of niobia/aluminas, which may be related to the Lewis acidity results. This shows that relatively strong acid–base pairs are required for methanol dehydration. On the other hand, the elimination of strongly basic hydroxyls by niobia deposition markedly decreased the inhibiting effect of carbon dioxide on the methanol dehydration activity.

In the direct production of DME from a mixture of carbon monoxide and hydrogen using a mixed system comprised of a methanol synthesis CuZnAl component and a dehydration component, the expected effect of the addition of the dehydration component on activity and selectivity was observed, but the overall activity was significantly larger with a niobia/alumina as the dehydration component than with the pure alumina. This is probably the result of the smaller inhibition of methanol dehydration by carbon dioxide, rendering more efficient the reaction cycle comprised of methanol synthesis, methanol dehydration and the WGS reaction.

Acknowledgments

To PETROBRAS for financial support to this project. To Agência Nacional do Petróleo, ANP, for a M.Sc. scholarship for A.M.F.

Appendix A. Supplementary data

Supplementary data associated with this article can be found, in the online version, at http://dx.doi.org/10.1016/j.cattod.2012.02.062.

References

[1] E.F. Sousa-Aguiar, L.G. Appel, C. Mota, Catalysis Today 101 (2005) 3–7.
[2] T.A. Semelsberger, R.L. Borup, H.L. Greene, Journal of Power Sources 156 (2006) 497–511.
[3] Q. Ge, Y. Huang, F. Qiu, S. Li, Applied Catalysis A 167 (1998) 23–30.
[4] R. Yang, X. Yu, Y. Zhang, W. Li, N. Tsubaki, Fuel 87 (2008) 443–450.
[5] J. Lee, K. Lee, S. Lee, Journal of Catalysis 144 (1993) 414–424.
[6] I. Wender, Fuel Processing Technology 48 (1996) 189–297.
[7] M. Xu, J.H. Lunsford, D.W. Goodman, A. Bhattacharyya, Applied Catalysis A 149 (1997) 289–301.
[8] Q. Sun, Y. Fu, H. Yang, A. Auroux, J. Shen, Journal of Molecular Catalysis A 275 (2007) 183–193.
[9] J. Khom-in, P. Praserthdam, J. Panpranot, O. Mekasuwandumrong, Catalysis Communications 9 (2008) 1955–1958.
[10] J. Fei, Z. Hou, B. Zhu, H. Lou, X. Zheng, Applied Catalysis A 304 (2006) 49–54.
[11] Y. Ohno, M. Yoshida, T. Shikada, O. Inokoshi, JFE Technical Report 8 (2006) 34–40.
[12] S. Lee, A. Sardesai, Topics in Catalysis 32 (2005) 197–207.
[13] J.-L. Li, X.-G. Zhang, T. Inui, Applied Catalysis A 147 (1996) 23–33.
[14] D. Mao, W. Yang, J. Xia, B. Zhang, Q. Song, Q. Chen, Journal of Catalysis 230 (2005) 140–149.
[15] D. Mao, W. Yang, J. Xia, B. Zhang, G. Lu, Journal of Molecular Catalysis A 250 (2006) 138–144.
[16] F.S. Ramos, A.M.D. de Farias, L.E.P. Borges, J.L. Monteiro, M.A. Fraga, E.F. Sousa-Aguiar, L.G. Appel, Catalysis Today 101 (2005) 39–44.
[17] Q. Xu, T. Li, Y. Yan, Journal of Fuel Chemistry and Technology 36 (2008) 176–180.
[18] M. Abdel Rehim, A.C.B. dos Santos, V.L. Camorim, A.C. Faro Jr., Applied Catalysis A 305 (2006) 211–218.
[19] L.J. Burcham, J. Datka, I.E. Wachs, Journal of Physical Chemistry B 103 (1999) 6015–6024.
[20] D. Bayot, B. Tinant, M. Devillers, Catalysis Today 78 (2003) 439–447.
[21] K. Asakura, Y. Iwasawa, Chemistry and Technology of Fuels and Oils 15 (1986) 859–862.
[22] J.B. Peri, Journal of Physical Chemistry 809 (1965) 220–230.
[23] H. Knözinger, P. Ratnasamy, Catalysis Review 17 (1978) 31–70.
[24] G. Busca, V. Lorenzelli, V.S. Escribano, R. Guidetti, Journal of Catalysis 131 (1991) 167–177.
[25] C. Morterra, G. Magnacca, Catalysis Today 27 (1996) 497–532.
[26] A.S. Rocha, A.M.S. Forrester, M.H.C. de la Cruz, C.T. da Silva, E.R. Lachter, Catalysis Communications 9 (2008) 1959–1965.
[27] C. Emeis, Journal of Catalysis 141 (1993) 347–354.
[28] K. Tanaka, A. Osaki, Journal of Catalysis 8 (1967) 1–7.
[29] G. Connell, J.A. Dumesic, Journal of Catalysis 105 (1987) 285–298.
[30] C.L.T. da Silva, V.L.L. Camorim, J.L. Zotin, M.L.R. Duarte Pereira, A.D.C. Faro, Catalysis Today 57 (2000) 209–217.
[31] M.I. Zaki, M.A. Hasan, F.A. Al-Sagheer, Colloids and Surfaces 190 (2001) 261–274.
[32] J.C. Lavalley, Catalysis Today 27 (1996) 377–401.
[33] J. Baltrusaitis, J.H. Jensen, V.H. Grassian, Journal of Physical Chemistry B 110 (2006) 12005–12016.
[34] A.M. Turek, I.E. Wachs, E. DeCanio, Journal of Physical Chemistry 96 (1992) 5000–5007.
[35] R.S. Schiffino, R.P. Merrill, Journal of Physical Chemistry 97 (1993) 6425–6435.
[36] S. Fujita, M. Usui, H. Ito, N. Takezawa, Journal of Catalysis 157 (1995) 403–413.
[37] Q. Sun, C.-W. Liu, W. Pan, Q.-M. Zhu, J.-F. Deng, Applied Catalysis A 171 (1998) 301–308.
[38] K. Klier, V. Chatikavanij, R.G. Herman, G.W. Simmons, Journal of Catalysis 74 (1982) 343–360.
[39] T. Ogawa, N. Inoue, T. Shikada, Y. Ohno, Journal of Natural Gas Chemistry 12 (2003) 219–227.